Eur. Phys. J. Special Topics **229**, 3537–3550 (2020)
© The Author(s) 2020
https://doi.org/10.1140/epjst/e2020-000102-4

THE EUROPEAN PHYSICAL JOURNAL SPECIAL TOPICS

Regular Article

Effects of the QCD phase transition on hadronic observables in relativistic hydrodynamic simulations of heavy-ion reactions in the FAIR/NICA energy regime

Christian Spieles[1,2,a] and Marcus Bleicher[1,2]

[1] Institut für Theoretische Physik, Goethe-Universität, Max-von-Laue-Strasse 1, 60438 Frankfurt am Main, Germany
[2] Helmholtz Research Academy Hesse for FAIR, Campus Frankfurt, Frankfurt, Germany

Received 31 May 2020 / Accepted 27 October 2020
Published online 21 December 2020

Abstract. We investigate hadronic particle spectra and flow characteristics of heavy-ion reactions in the FAIR/NICA energy range of 1 AGeV $\leq E_{\mathrm{lab}} \leq$ 10 AGeV within a relativistic ideal hydrodynamic one-fluid approach. The particlization is realized by sampling the Cooper-Frye distribution for a grand canonical hadron gas on a hypersurface of constant energy density. Results of the hydrodynamic calculations for different underlying equations of state are presented and compared with experimental data and microscopic transport simulations. The sensitivity of the approach to physical model inputs concerning the initial state and the particlization is studied.

1 Introduction

The exploration of the phase structure of the theory of strong interaction or Quantum Chromodynamics (QCD) has been one of the major goals of relativistic nuclear physics during the last 30 years [1]. Especially the programs at the AGS (EOS collaboration [2]) and at CERN's SPS (NA49 [3], and Shine collaboration [4]) and later the RHIC-BES program (STAR collaboration [5]) have tried to to find unambiguous signals for the onset of deconfinement. On the experimental side this search will continue in the next years with the novel facilities in Darmstadt and Dubna, namely the FAIR project [6] and the NICA project [7]. One the theoretical side, the search for the onset of deconfinement is plagued by the lack of quantitative predictions and high quality numerical simulations for a collision with a QCD phase transition [8]. While this might sound surprising, it is unfortunately a fact that most transport simulations for heavy ion collisions in the FAIR/NICA regime do not allow to include a phase transition and can therefore at best provide the background dynamics [9] (a notable exception is [10]).

[a] e-mail: spieles@itp.uni-frankfurt.de

In contrast, relativistic hydrodynamics simulations can provide new insights by incorporating a phase transition at finite baryo-chemical potential as needed for this energy. The application of hydrodynamic models to the simulations of nuclear collisions has a long history [11–16]. The strength of this approach lies in the fact that apart from the basic model assumption of local thermal equilibrium essentially only the choice of a concrete equation of state enters as a physical input.

At low energies, the hydrodynamic picture of a single fluid describing the interaction of projectile and target nuclei has been used early on to study collective effects like directed flow and the dependence of these effects on the nuclear equation of state (see, e.g. [14,15,17]). Spectra of secondary particles, however, have rarely been analyzed in a purely hydrodynamic description of low energy heavy ion collisions, a notable exception being the two-fluid model approach of [18].

At high collision energies, on the other hand, hydrodynamic models have been found appropriate for the description of the hot and essentially baryon free matter created at top RHIC and LHC energies. Especially since the start of the experimental program at RHIC in 2000, one-fluid hydrodynamics has seen a tremendous increase in its applications to relativistic heavy ion collisions [19,20].

In addition to pure one-fluid hydrodynamics, alternative approaches have been developed, namely two- and three-fluid hydrodynamics and Boltzmann+Hydro hybrid models. Here, the initial stage consisting of the target at projectile nucleons is treated separately from the created fireball. This allows to include the strongly anisotropic momentum distribution of the initial stage and to include a phase transition for the central reactions stages. Especially at intermediate energies where the initial baryon currents can be separated in momentum space such approaches are very valuable. Prime examples for three fluid hydrodynamics models are [21–24], while the idea of coupled Boltzmann+Hydro simulations was pioneered in [25–29] and later applied in [30–33].

A major drawback of hybrid and multi-fluid approaches is that they typically rely on a separation (in space and momentum space) of the baryon currents. Especially at low energies this assumption might not be fulfilled and the different currents (propagated in different fluids) should be treated as a single thermodynamic system at each space time point. The typical minimal scale from which on a simple multi-fluid approach without unification of the fluids can be used is provided by the thermal velocity in a typical cell in relation to the Moeller velocity between the fluids (or baryon currents). This was studied in [22] and indicates that even up to 11 AGeV one-fluid hydrodynamics provides a good approximation to the expansion stage of the reaction.

In the present study, a relativistic ideal one-fluid model of heavy-ion collisions is applied to the FAIR/NICA energy regime. The reaction dynamics is described hydrodynamically starting from cold projectile and target nuclei up to the particlization into hadrons. The final m_t spectra of protons, pions and kaons from central Au+Au collisions are systematically analyzed and compared with experimental data for different equations of state and for different beam energies. Excitation functions of the flow parameters v_1 and v_2 in mid-central collisions are also studied. A special focus is laid on the importance of initial state density fluctuations for these observables.

2 The model

2.1 Initialization

The model can either be initialized with averaged nuclear profiles of the nucleons in each projectile and target nucleus or using a Monte Carlo procedure to

provide fluctuating initial stages for event-by-event simulations. Consequently, in the 'event-by-event' mode multiple hydrodynamic events with different initial states are calculated in order to obtain a sample of final states which are then averaged for the present study. While in the 'averaged' mode initial configurations are first averaged and the a single hydrodynamic evolution is performed. Thus, the 'averaged' mode neglects initial stage fluctuations and leads in general to smoother initial density and energy profiles. The practical implementation of the fluid initialization follows [29]: The spatial coordinates of the nucleons from an individual initial state is replaced by three-dimensional Lorentz-contracted Gaussians of width $\sigma = 1$ fm. The resulting sum of the corresponding energy, momentum and baryon-densities of all nucleons is then mapped on the spatial grid with cell-size $(0.2\text{ fm})^3$. The hydrodynamic evolution thus starts directly at $t = 0$ with the center of both cold nuclei being at a distance $\Delta z = r_1 + r_2$, with z being the longitudinal direction and r_i being the radius of nucleus i.

2.2 Equations of motion

Ideal relativistic hydrodynamic assumes conservation of energy, momentum and charges:

$$\partial_\mu T^{\mu\nu} = 0 \quad \text{and} \quad \partial_\mu N^\mu = 0. \tag{1}$$

Here, $T^{\mu\nu}$ is the energy-momentum tensor and N^μ is the baryon four-current. These quantities can be expressed in terms of the fluid's four-velocity u^μ and the thermodynamic state in the local restframe of the fluid, described by the energy density ϵ, the pressure p and the baryon density n:

$$T^{\mu\nu} = (\epsilon + p)u^\mu u^\nu - pg^{\mu\nu} \quad \text{and} \quad N^\mu = nu^\mu. \tag{2}$$

In addition to the hydrodynamic equations, a specific equation of state of the matter is required in the form $p = p(\epsilon, n)$. The following coupled equations then determine the time evolution of the system:

$$\partial_t T^{00} + \boldsymbol{\nabla} \cdot (T^{00}\boldsymbol{v}) = -\boldsymbol{\nabla} \cdot (p\boldsymbol{v}), \tag{3}$$

$$\partial_t T^{0i} + \partial_i(\sum T^{0j} v_j) = -\partial_i p \quad \text{for} \quad i = 1, 2, 3, \tag{4}$$

$$\partial_t N^0 + \boldsymbol{\nabla} \cdot (N^0\boldsymbol{v})) = 0. \tag{5}$$

These equations are numerically solved with the SHASTA algorithm [34,35]. In each time step, the algorithm consistently links the discretized conserved quantities T^{00}, T^{0i} and N^0 (given in the calculational frame) with the pressure p (given in the local rest frame) and the fluid's three-velocity $\boldsymbol{v}$ of each cell.

A main advantage of the SHASTA as compared to other approaches is its ability to handle shock wave formation and propagation by the flux corrected transport with non-linear feedback [36]. Especially for our application at low energies, this is a crucial feature, because the entropy production in the initial stage is completely described by shock wave formation.

2.3 Equations of state

The Equation of State (EoS) is the main ingredient into the hydrodynamic simulation. At high energies, i.e. for systems with (nearly) vanishing net-baryon density the EoS

can be obtained from fits to lattice QCD calculations [37,38], at low energies with high baryo-chemical potentials lattice QCD calculations can unfortunately not provide ab-initio results for the EoS and one has to rely on phenomenological approaches that converge to lattice QCD results in certain limits. For the present study, different equations of state have been assumed: The *hadron gas* is an ideal relativistic quantum-gas of known baryon and meson resonances up to ≈ 2 GeV. It reflects the same degrees of freedom as the hadronic cascade model UrQMD. For details, we refer to [39]. The *MIT bag model* equation of state and its implication on fluid-dynamic properties have been discussed in [35]. This (rather schematic) equation of state assumes a version of the $\sigma - \omega$-model for the hadronic phase and a non-interacting gas of massless u and d quarks and gluons confined by a bag pressure for the QGP phase. The transition between the two phases is of first-order, governed by the Gibbs condition. The bag model EoS serves mainly to showcase the most drastic effects of a phase transition. According to the *chiral model* [40], strange and non-strange baryons interact via mesonic mean-fields. This model equation of state exhibits a cross-over phase transition to deconfined matter.

Figure 1 depicts the three equations of state for three different fixed values of net-baryon density n. Shown is the pressure as a function of energy density. This is the hydrodynamically relevant representation of the equation of state, since the pressure can be regarded as the 'response' of the matter for a given condition (baryon density and energy density) the system is forced into in the course of the evolution. Obviously, the different model equations of state indicate strongly differing thermodynamic behaviour of nuclear matter. It will be shown below, how this reflects in the outcome of the different hydrodynamic simulations.

2.4 Hadronic freeze-out

The transition between the fluid phase and the microscopic transport description of the reaction is given by the Cooper-Frye equation [41]:

$$E\frac{dN_i}{d^3p} = \int_\sigma f_i(x,p)p^\mu d\sigma_\mu. \tag{6}$$

f_i denotes the particle distribution function of hadron species i, boosted according to the fluid velocity of the hypersurface element.

The hydrodynamic freeze-out or particlization takes place on a hypersurface of equal local energy density ϵ_{fr} of the fluid. The numerical procedure for determining the hypersurface is described in [42]. In the present study, reaching nuclear ground state energy density is used as the particlization criterion, i.e. the value of local energy density where the hydrodynamic fields are converted into hadrons is $\epsilon_{\mathrm{fr}} = \epsilon_0$. The duration of the hydrodynamic evolution until Cooper-Frye freeze-out depends somewhat on the equation of state and the collision energy, but of course also on rapidity. For the present study, typical values of the average freeze-out time, weighted with the entropy flow through the hyper-surface, are on the order of $10 - 15$ fm/c.

Hadrons are sampled according to the grand-canonical description of a non-interacting relativistic hadron gas in equilibrium, taking into account the same degrees of freedom as the microscopic transport model UrQMD. The values of T and μ_B depend on the baryon density of the fluid at the particular hypersurface element. Different to the implementation of [29], the conservation of energy and baryon number in the grand-canonical ensemble refers to expectation values, not to individual events. Electric charges are not propagated explicitly in the hydrodynamic simulation. In order to recover the net-charge of the initial state of the heavy-ion collision in the final state, the Z/A ratio of the system is used as global constraint which

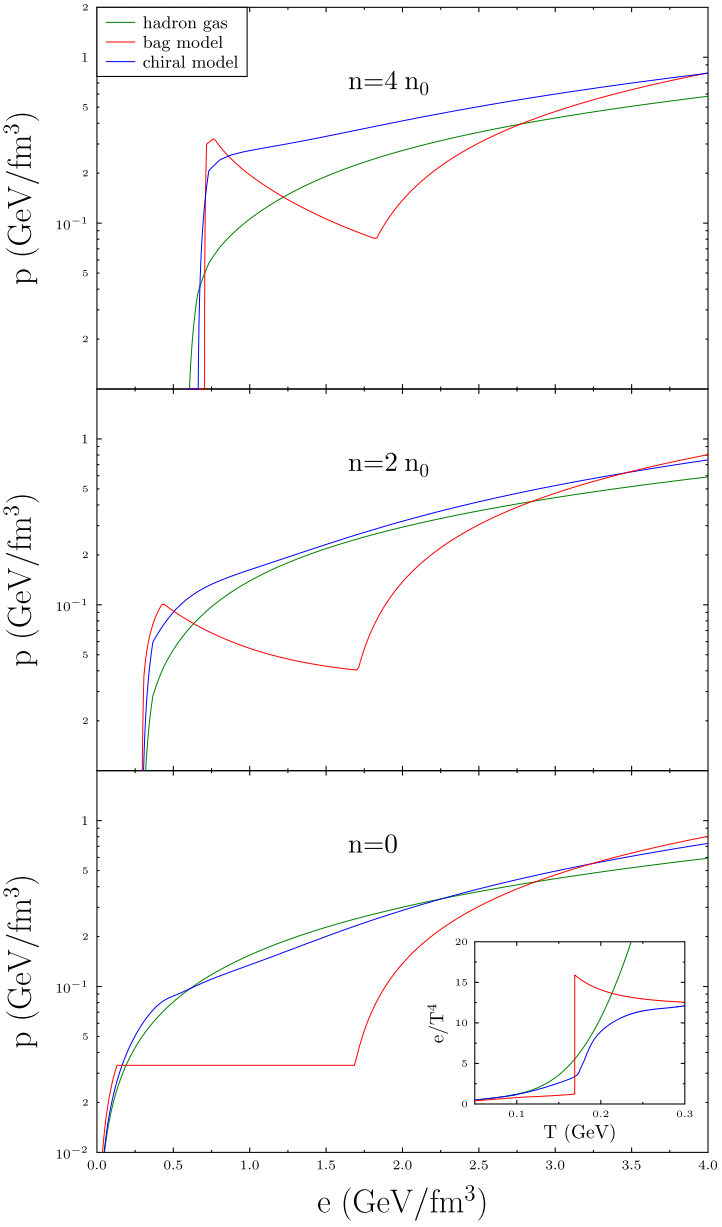

Fig. 1. Equations of state employed in the hydrodynamic model simulations. Shown is the pressure p as a function of energy density e for different fixed values of net-baryon density n (n_0 is the net-baryon density of the nuclear ground state). The inset in the bottom figure displays the dimensionless quantity e/T^4 as a function of T for the case $n = 0$.

implies a certain isospin asymmetry for each element of the freeze-out hypersurface, depending on the local values of T and μ_B. The sampling of particles then takes into account this isospin asymmetry.

In principle, there should be no need for an additional normalization of the particle yields, since the sampling procedure runs over all elements of the particlization

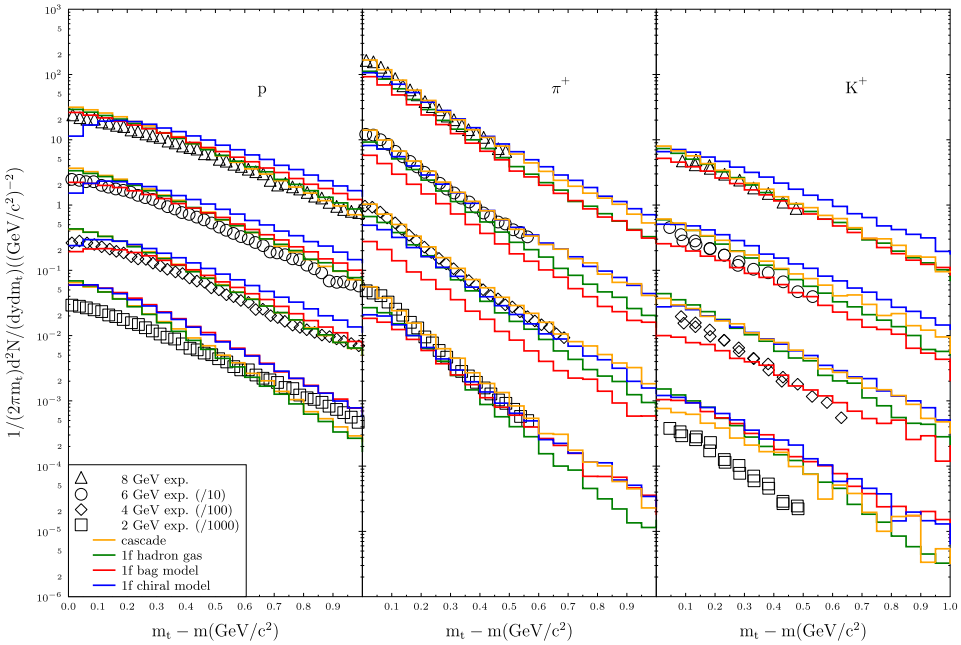

Fig. 2. Invariant particle yield at $|y - y_{cm}| < 0.05$ as a function of $m_t - m_0$ in central Au+Au collisions at (2, 4, 6, and 8) AGeV. Shown are experimental data for protons from E895 [43], for π^+ from E895 [44] and for K^+ from E866 and E917 [45] in comparison with different hydrodynamic simulations and the UrQMD cascade model.

hypersurface. Indeed, the 'raw' model-outcome is consistent with baryon number conservation on a 1% level in the case of the hadron gas equation of state and assuming an averaged initial state. Taking into account initial state fluctuations reduces the agreement to a 5% level. Equations of state other than the ideal hadron gas in some cases lead to even larger apparent violations of baryon number conservation. Therefore, we calculate an overall correction factor for the net-baryon number expectation value of each individual particlization hypersurface and apply it in the sampling procedure (for all hadron species).

The transition from the hydrodynamic evolution is followed by final state interactions (scattering and decays). For these, the UrQMD-cascade description is employed, as in [29–33]. However, since the particlization is assumed to take place at significantly lower energy densities, the hadronic scatterings at this late stage are not relevant for any observables analyzed in this study.

3 Results

3.1 Hadronic particle spectra

Figure 2 shows transverse mass spectra of protons, π^+ and K^+ at midrapidity for central Au+Au collisions at different energies. In the simulations, the impact parameter is set to $b = 2$ fm, whereas the experimental data represent the 5% most central events. Hydrodynamic simulations using the three different equations of state are compared with the microscopic UrQMD model and experimental data from [43–45]. Firstly, one notes a close similarity between the hydrodynamic simulation using the

hadron gas equation of state and the microscopic transport model for all hadron species at all energies. This is a surprising fact, given that the hydrodynamic model comes with extremely few free parameters, none of which is fitted to experimental data from heavy ion reactions. The final state of the hydrodynamic description only reflects local energy and momentum conservation in combination with the assumption of immediate local equilibration of all hadronic degrees of freedom at all times. The microscopic model, on the other hand, goes to great length to take into account the non-equilibrium physics of a nuclear collision by implementing hundreds of elementary cross sections and decay channels. However, the fundamentally different models show quantitatively very similar amounts of nuclear flow (indicated by the slope of the protons), as well as entropy and strangeness production (yield and slope of the pions and kaons, respectively).

There are some significant differences between the simulations with different equations of state, though. Firstly, the chiral model equation of state shows the strongest flow, indicated by relatively flat slopes of protons, and also secondaries, in particular at higher energies. This corresponds to the relatively high values of pressure at given baryon density in a wide range of energy densities, see Figure 1. The bag model exhibits interesting deviations from the other scenarios, concerning the pion and kaon yields at 4 AGeV, which appear clearly suppressed. This can be understood in view of the low pressure (and relatively low temperature) in the mixed phase, which seems to dominate the reaction dynamics just at 4 AGeV (at this energy also fluctuations due to spinodal instabilities reach their maximum [46]). At 2 AGeV it is plausible that only a small portion of the reaction volume enters the mixed phase of the equation of state.

The comparison with experiment shows that UrQMD and the hydrodynamic calculations with all inspected equations of state do not fully capture the flow in the slope of the proton spectrum at 2 AGeV. At 4–8 AGeV, both the hydrodynamic models as well as the UrQMD model agree nicely with the proton data, perhaps with the exception of the chiral model equation of state which renders slightly too much transverse collective motion. The spectra of pions are well reproduced by hydrodynamics at all energies. As mentioned above, the bag model equation exhibits a remarkable deviation from the other model scenarios at intermediate energies, most pronounced at 4 AGeV. Hence, the outcome of the bag model model equation of state is also clearly in conflict with experimental data.

All models presented here fail to reproduce the kaon yield at 2 AGeV and 4 AGeV. It appears that the steep rise of the K/π ratio when comparing 4 AGeV collisions with 2 AGeV poses a challenge for dynamical model descriptions of hadron production in heavy-ion collisions. Statistical models with an assumed energy dependence of the thermodynamical parameters describe the observed strangeness production [47]. However, new complications arise for most models when trying to explain experimental data at higher collision energies [48].

As for the present analysis, in particular the hadron gas equation of state shows very good agreement with the experimental data for all hadron species at 6 and 8 AGeV. It seems that these collision energies with significantly higher collision rates and hadron production cross sections way above threshold are consistent with the assumption of thermal and hadrochemical equilibrium during the determining reaction stage.

As mentioned above, apart from the equation of state, the hydrodynamic model does not leave much space for different physical model parameters or assumptions that could affect the outcome. In the following, the sensitivity of the hadron spectra to this model input is analyzed. Firstly, one might question the assumed initial state of the fluid as being determined by the distribution of a finite number of nucleons on the computational grid. It could be argued that averaging density fluctuations over an ensemble of projectile and target nuclei constitute the appropriate initial

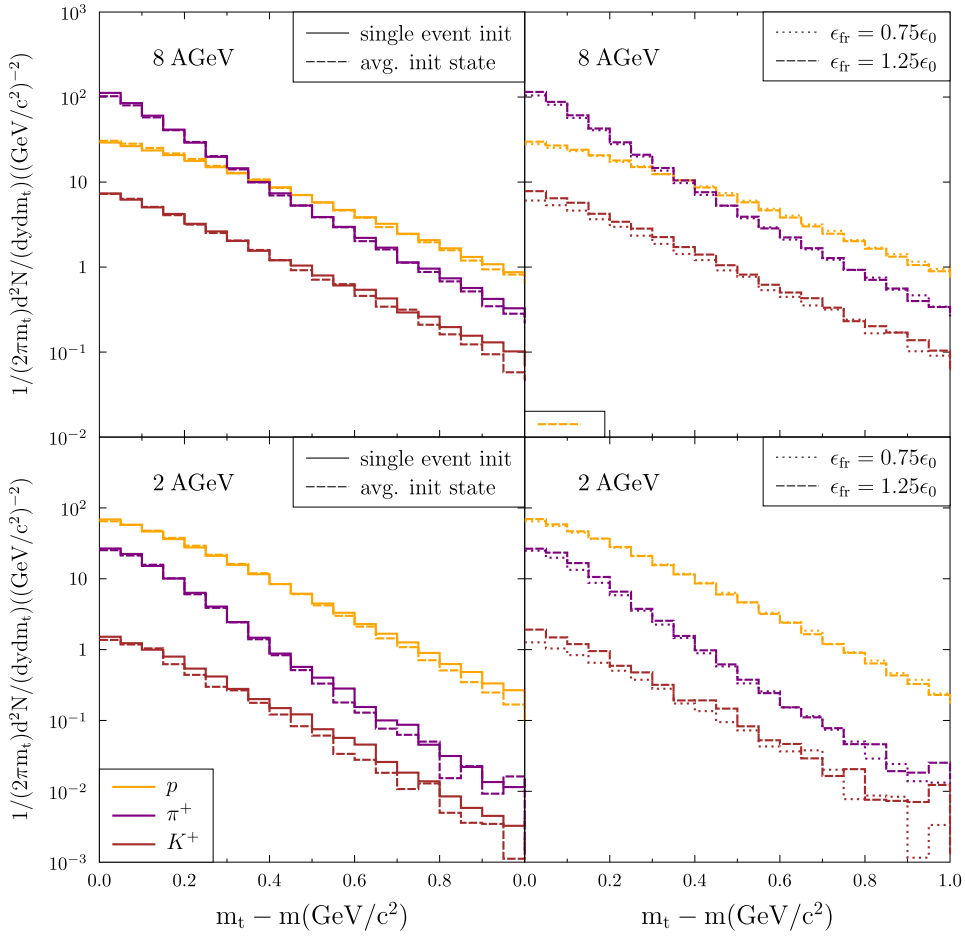

Fig. 3. Invariant particle yield at $|y - y_{cm}| < 0.05$ as a function of $m_t - m_0$ in central Au+Au collisions at 2 and 8 AGeV according to the hydrodynamic calculation with the hadron gas equation of state. Shown are the sensitivities with respect to initial state density fluctuations (left hand side) and with respect to the value of the particlization parameter ϵ_{fr} (right hand side).

state for the fluid dynamical description. In Figure 3, the plots on the left hand side show an analysis of the hadron spectra for the standard scenario with initial state density flucutations in comparison with the scenario with an averaged initial state. The resulting m_T distribution of all particle species are only very weakly sensitive to the choice of the initial state scenario ('averaged' initial conditions vs. 'event-by-event' initial conditions). This holds for the whole energy range explore in this study.

Next we explore the transition criterion from the hydrodynamic stage to the Boltzmann dynamics. The parameter ϵ_{fr}, the value of the energy density that serves as the hydrodynamic freeze-out or particlization criterion. For the present study, the value is set to $\epsilon_{fr} = \epsilon_0$, the energy density of the nuclear ground state. This value is motivated by the typical mean free path of the nucleons and may be seen as a lower limit for this value. In contrast, in [29], a value of $\epsilon_{fr} = 5\epsilon_0$ was assumed for collisions in the highly relativistic regime. However, this is not appropriate for the

present study where such an energy density may not even be reached as a peak value. To be consistent, the energy density where particlization takes place is instead chosen such that cold nuclei are below or just at the threshold of the fluid description. Much lower values of $\epsilon_{\rm fr}$, on the other hand, can hardly be justified due to the resulting large mean free path or low scattering rates. Thus, the reasonable parameter range of $\epsilon_{\rm fr}$ is rather small for low energy nuclear collisions. Still, the sensitivity of the the model on its variation should be checked. In Figure 3, the plots on the right hand side show an analysis of the hadron spectra for $\epsilon_{\rm fr} = 0.75\epsilon_0$ in comparison with $\epsilon_{\rm fr} = 1.25\epsilon_0$. The spectra from the hydrodynamic model calculations are very robust with respect to the changes of $\epsilon_{\rm fr}$ in this range. One just observes a slight suppression of kaon production for the lower value of $\epsilon_{\rm fr}$, which is to be expected considering the lower average freeze-out temperatures associated with this choice of $\epsilon_{\rm fr}$.

3.2 Directed flow

Excitation functions of the directed flow have been studied in [17] as a possible way of probing the equation of state of nuclear matter in a fluid-dynamic model. These calculations did not take into account hadronic freeze-out – as most of the early studies – and relied directly on the analysis of the energy momentum tensor of the baryonic fluid. The proposed quantity for measuring the effect was the mean x component of the fluid momentum (with x pointing transversely in the reaction-plane), integrated over forward rapidity and weighted with the baryon number rapidity density. Unfortunately, this is not an experimentally accessible observable.

In the present study, the directed flow is calculated on the basis of the nucleons after particlization and subsequent hadronic freeze-out from the final microscopic transport stage. The directed flow is quantified by the first Fourier coefficient of the azimuthal distribution of the nucleons with respect to the event plane:

$$v_1 = \langle \cos(\phi) \rangle = \left\langle \frac{p_x}{p_T} \right\rangle . \tag{7}$$

The value of v_1 of particle distributions changes its sign at midrapidity for symmetry reasons. Therefore, in order to define a meaningful observable integrated over rapidity[1], the quantitity $\langle v_1 \mathrm{sgn}(y) \rangle$, averaging over all individual nucleons, is considered. This quantity, called the directed flow, is depicted in Figure 4 as a function of beam energy for different model equations of state.

The UrQMD cascade calculation may serve as a baseline to which the different hydrodynamic simulations are compared. The energy dependence of the directed flow is rather weak. One observes a slow decrease which seems to saturate at a value lower than all fluid-dynamic model scenarios. For the hydrodynamical calculation with a hadronic equation of state with the same degrees of freedom as the UrQMD model, the directed flow effect is also rather weak and the energy dependence is not very pronounced. While, this scenario exhibits a slow increase of the directed flow parameter instead of a decrease, the numerical values of the directed flow are rather similar for both hadronic scenarios.

In contrast, the chiral model equation of state shows a completely different energy dependence of the directed flow: Firstly, the flow effect is stronger at all energies. Secondly, it exhibits a pronounced maximum at around 4 AGeV. In contrast, the bag model equation of state renders the minimum of the directed flow at around 6 AGeV which perfectly coincides with the results of [17], where this minimum had

[1] An alternative observable may be defined by the slope of v_1 at midrapidity. However, the extraction of a slope parameter is less reliable than an integrated value.

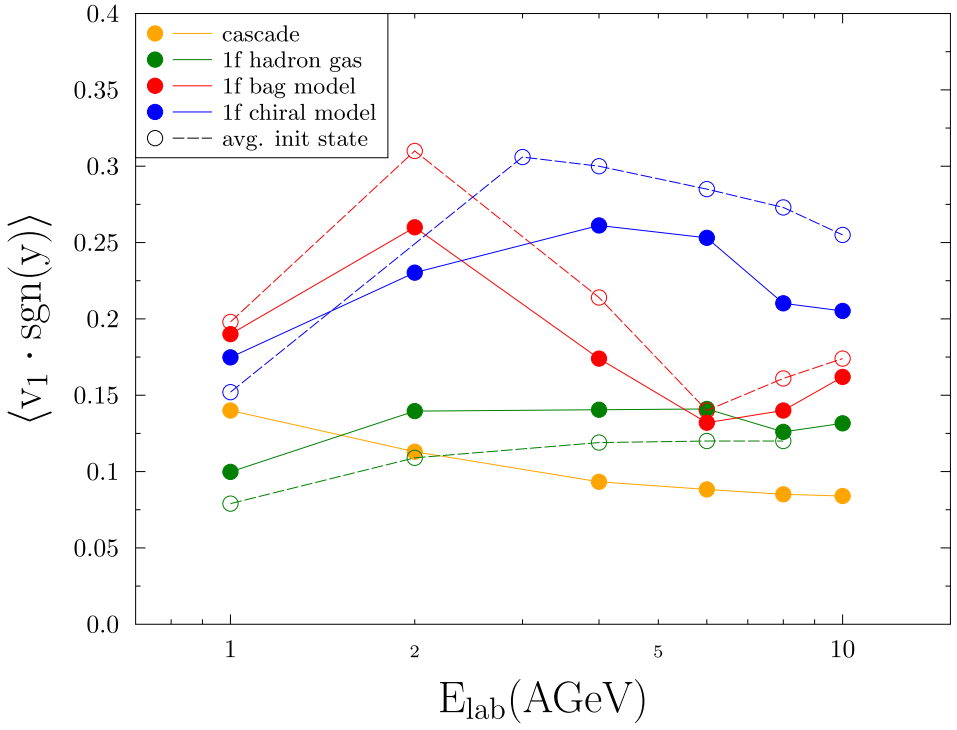

Fig. 4. Mean directed transverse momentum in the reaction plane for protons in Au+Au collisions ($b = 7$ fm) at different energies. Shown are the results of hydrodynamic calculations for different equations of state with and without taking into account initial state fluctuations of the nuclear matter distributions. Also shown is the result of the microscopic UrQMD transport simulation.

been proposed as a qualitative signal for the transition of hadronic matter to quark and gluon degrees of freedom. The reason is, of course, the extreme softening of the equation of state in the mixed phase, as can bee seen from Figure 1. It is notable that the chiral model also incorporates a phase transition to deconfined matter with quark degrees of freedom, which is best recognizable in the inset of Figure 1 as $e/T^4(T)$. However, assuming this equation of state does not lead to the minimum in the directed flow in the inspected energy range.

As mentioned above, the values of the pressure for given baryon and energy density determine the hydrodynamic evolution. In this respect, the differences between the chiral model equation of state and the bag model of state are much more pronounced than the differences between the chiral model and the hadron gas over a considerable range of energy density and baryon density. This explains the differences of the directed flow parameter between 2 and 8 AGeV. For low beam energies between 1 and 2 AGeV, on the other hand, the chiral model and the bag model equation of state show very similar amounts of directed flow, whereas the hadron gas differs considerably. This seems plausible in view of the Figure 1 (centre and top), where the pressure of nuclear matter for energy densities and baryon densities expected in heavy-ion collisions at these energies can be read off. The hadron gas with its numerous noninteracting degrees of freedom shows much lower values of pressure than both the bag model and chiral model.

For the hydrodynamic model Figure 4 also shows the resulting directed flow parameters according to the scenario with the 'averaged' initial state, where density

fluctuations of single events are averaged over. In this case, the effect of directed flow is consistently stronger than in the standard scenarios. The momentum correlations corresponding to the directed flow appear to be distorted by random fluctuations of the spatial fluid distribution. The importance of the initial state fluctuations was also observed in [49].

3.3 Elliptic flow

Finally, we turn to the elliptic flow or v_2. The elliptic flow is quantified by the second Fourier coefficient of the azimuthal distribution of the nucleons with respect to the event plane:

$$v_2 = \langle \cos(2\phi) \rangle = \left\langle \frac{p_x^2 - p_y^2}{p_x^2 + p_y^2} \right\rangle . \tag{8}$$

The experimentally observed elliptic flow of protons at midrapidity for mid-central Au+Au collisions in the beam energy range between 1 and 10 AGeV exhibits a characteristic sign change [50]. The elliptic flow is especially important, as it provides an extremely sensitive link to the Equation of State as discussed in [51]. In Figure 5 the experimental excitation function of v_2 is compared to the hydrodynamic model for different equations of state and to the UrQMD calculation. The impact parameter in the simulations is $b = 7$ fm.

For the UrQMD cascade simulation, one observes the correct trend of the elliptic flow as a function of energy, namely an increase from negative to positive values, however, the absolute values of the flow parameter v_2 are significantly lower than the experimental data. This is consistent with the findings of [51,52] where it was demonstrated that the additional assumption of a hard equation of state (or a soft EoS with momentum dependence) is needed in order to describe the elliptic flow with the microscopic UrQMD model. A cascade of on-shell nucleons and secondaries scattering according to unmodified cross sections apparently does not create the observed flow characteristic [51].

The results for the hydrodynamic simulation with the hadron gas equation of state do not show a sign change of the elliptic flow parameter. In fact, v_2 is positive at all energies and it is significantly higher than the experimental data. The lack of the 'squeeze-out' effect at low energies is plausible, since the hadron gas equation of state is very soft at low values of energy and baryon density (see Fig. 1). Of all hydrodynamic scenarios, the excitation function of the elliptic flow rendered by the chiral model equation of state exhibits the best agreement with the experimental curve. The bag model equation of state, on the other hand, 'exaggerates' the actual trend of the elliptic flow. The sign change is reproduced, but the absolute negative and positive values are significantly larger. The reason for this behavior – as compared to the chiral model – can be explained in terms of the equations of state as shown in Figure 1: The strong squeeze-out effect can be attributed to the relative stiffness of the bag model equation of state in the purely hadronic phase. The extreme softness of the bag model equation of state in the mixed phase, on the other hand, is related to a delayed expansion, which clearly favors positive elliptic flow due to the absence of spectator matter during the expansion phase.

Again, we contrast the 'event-by-event' simulations with the calculations employing 'averaged' initial conditions, shown in Figure 5 as open symbols. As in the case of the directed flow, the (positive or negative) elliptic flow effects in the 'averaged' scenario are stronger than for the more realistic scenario with fluctuating initial state

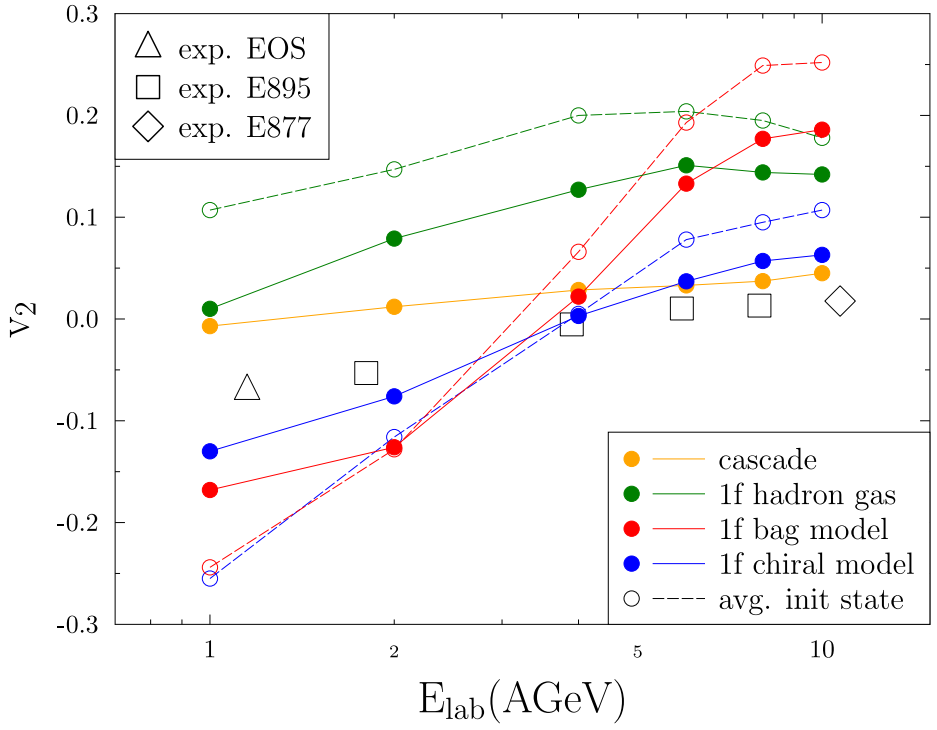

Fig. 5. Excitation function of the elliptic flow v_2 of protons at $|y - y_{cm}| < 0.05$ in Au+Au collisions ($b = 7$ fm). Shown are hydrodynamic calculations with different equations of state, the results of the microscopic transport model UrQMD and experimental data from [50]. Also shown are the hydrodynamic results without taking into account initital state density fluctuations.

configurations. We conclude that fluctuating initial conditions and a realistic EoS with a transition to a QGP can best describe the flow data in this energy regime.

4 Summary and conclusion

We have revisited the one-fluid description of nuclear collisions for the low energy regime. To this aim, we used a SHASTA implementation of ideal relativistic one-fluid hydrodynamics in order to study central Au+Au reactions in the beam energy range between 1 and 10 AGeV. By applying a relativistically invariant particlization scheme with conservation of average energy, net-baryon number and charge, we extracted final state samples of individual hadrons. The resulting m_t spectra of protons, π^+ and K^+ at midrapidity depend to some extent on the assumed equation of state. Very good agreement with experimental data is observed for the hadron gas equation of state and $E_{\rm lab}$ between 6 and 10 AGeV. However, the spectra from the hydrodynamic model scenarios are remarkably similar to the microscopic UrQMD model results at all energies and for all particle species. The sensitivity of the hydrodynamic model to the value of the local energy density $\epsilon_{\rm fr}$ which defines the particlization hypersurface, is found to be very weak.

First and second flow harmonics of protons were analyzed and found to be much more sensitive to the Equation of State than inclusive particle spectra. The comparison to the experimental data indicates that the v_2 data can be best described with a chiral euqation of state that includes a phase transition to the QGP. In addition, we explored the effect of single-event density fluctuations of the initial state on the flow observables v_1 and v_2. We found that averaged initial stages do not allow for a realistic description of the flow data.

In view of the above results we conclude that the relativistic one-fluid hydrodynamic approach with particlization constitutes a useful baseline to predict and explore effects of the QCD phase transition in the FAIR/NICA energy range. Especially the improved EoS's, the fluctuating initial conditions and the state-of-the-art Monte Carlo freeze-out/transition procedure improve the results and reliability of the current one-fluid models over their ancestors.

Open Access funding enabled and organized by Projekt DEAL. This work was supported by the Helmholtz International Center for FAIR within the framework of the LOEWE program launched by the State of Hesse. The computational resources were provided by the Center for Scientific Computing (CSC) of the Goethe University Frankfurt. This work has been supported by COST Action THOR (CA15213).

Open Access This is an open access article distributed under the terms of the Creative Commons Attribution License (https://creativecommons.org/licenses/by/4.0), which permits unrestricted use, distribution, and reproduction in any medium, provided the original work is properly cited.

Publisher's Note The EPJ Publishers remain neutral with regard to jurisdictional claims in published maps and institutional affiliations.

References

1. S.A. Bass, M. Gyulassy, H. Stöcker, W. Greiner, J. Phys. G **25**, R1 (1999)
2. R.P. Scharenberg et al., Phys. Rev. C **64**, 054602 (2001)
3. K. Grebieszkow, Nucl. Phys. A **830**, 547C (2009)
4. L. Turko, Universe **4**, 52 (2018)
5. J. Adam et al., arXiv:2001.02852 [nucl-ex] (2020)
6. P. Senger, Int. J. Mod. Phys. E **29**, 2030001 (2020)
7. V.D. Kekelidze, JINST **12**, C06012 (2017)
8. I.C. Arsene, L.V. Bravina, W. Cassing, Yu.B. Ivanov, A. Larionov, J. Randrup, V.N. Russkikh, V.D. Toneev, G. Zeeb, D. Zschiesche, Phys. Rev. C **75**, 034902 (2007)
9. A. Ono et al., Phys. Rev. C **100**, 044617 (2019)
10. E.L. Bratkovskaya, W. Cassing, V.P. Konchakovski, O. Linnyk, Nucl. Phys. A **856**, 162 (2011)
11. S.Z. Belenkij, L.D. Landau, Nuovo Cim. Suppl. **3S10**, 15 (1956)
12. S.Z. Belenkij, L.D. Landau, Usp. Fiz. Nauk. **56**, 309 (1955)
13. A.A. Amsden, G.F. Bertsch, F.H. Harlow, J.R. Nix, Phys. Rev. Lett. **35**, 905 (1975)
14. C.Y. Wong, J.A. Maruhn, T.A. Welton, Nucl. Phys. A **253**, 469 (1975)
15. L.P. Csernai, B. Lukacs, J. Zimanyi, Lett. Nuovo Cim. **27**, 111 (1980)
16. I.N. Mishustin, V.N. Russkikh, L.M. Satarov, Relativistic heavy ion collisions within two-fluid dynamics, in *Proceedings of the 18th international International Symposium on Multiparticle Dynamics* (World Scientific Pub. Co., United States 987), pp. 473–480
17. D.H. Rischke, Y. Pürsün, J.A. Maruhn, H. Stöcker, W. Greiner, Acta Phys. Hung. A **1**, 309 (1995)
18. V.N. Russkikh, Y.B. Ivanov, Y.E. Pokrovsky, H.P. A, Nucl. Phys. A **572**, 749 (1994)

19. P. Huovinen, P.F. Kolb, U.W. Heinz, P.V. Ruuskanen, S.A. Voloshin, Phys. Lett. B **503**, 58 (2001)
20. Y. Zhou, W. Zhao, K. Murase, H. Song, One fluid might not rule them all, in *28th International Conference on Ultrarelativistic Nucleus-Nucleus Collisions (Quark Matter 2019) 4-9 November 2019, Wuhan, China,* (2020)
21. U. Katscher, D.H. Rischke, J.A. Maruhn, W. Greiner, I.N. Mishustin, L.M. Satarov, Z. Phys. A **346**, 209 (1993)
22. J. Brachmann, A. Dumitru, J.A. Maruhn, H. Stöcker, W. Greiner, D.H. Rischke, Nucl. Phys. A **619**, 391 (1997)
23. Yu.B. Ivanov, V.N. Russkikh, V.D. Toneev, Phys. Rev. C **73**, 044904 (2006)
24. P. Batyuk, D. Blaschke, M. Bleicher, Yu.B. Ivanov, I. Karpenko, S. Merts, M. Nahrgang, H. Petersen, O. Rogachevsky, Phys. Rev. C **94**, 044917 (2016)
25. A. Dumitru, S.A. Bass, M. Bleicher, H. Stöcker, W. Greiner, Phys. Lett. B **460**, 411 (1999)
26. S.A. Bass, A. Dumitru, M. Bleicher, L. Bravina, E. Zabrodin, H. Stöcker, W. Greiner, Phys. Rev. C **60**, 021902 (1999)
27. D. Teaney, J. Lauret, E.V. Shuryak, arXiv:nucl-th/0011058 (2001)
28. J. Steinheimer, M. Bleicher, H. Petersen, S. Schramm, H. Stöcker, D. Zschiesche, Phys. Rev. C **77**, 034901 (2008)
29. H. Petersen, J. Steinheimer, G. Burau, M. Bleicher, H. Stöcker, Phys. Rev. C **78**, 044901 (2008)
30. K. Werner, I. Karpenko, T. Pierog, M. Bleicher, K. Mikhailov, Phys. Rev. C **82**, 044904 (2010)
31. H. Song, S.A. Bass, U. Heinz, Phys. Rev. C **83**, 054912 (2011)
32. H. Song, S.A. Bass, U. Heinz, Erratum: Phys. Rev. C **87**, 019902 (2013)
33. G.S. Denicol, C. Gale, S. Jeon, A. Monnai, B. Schenke, C. Shen, Phys. Rev. C **98**, 034916 (2018)
34. D.H. Rischke, S. Bernard, J.A. Maruhn, Nucl. Phys. A **595**, 346 (1995)
35. D.H. Rischke, Y. Pürsün, J.A. Maruhn, Nucl. Phys. A **595**, 383 (1995)
36. G. Ben-Dor, *Handbook of Shock Waves* (Academic Press, San Diego, 2001)
37. P. Huovinen, P. Petreczky, Nucl. Phys. A **837**, 26 (2010)
38. A. Monnai, B. Schenke, C. Shen, Phys. Rev. C **100**, 024907 (2019)
39. D. Zschiesche, S. Schramm, J. Schaffner-Bielich, H. Stöcker, W. Greiner, Phys. Lett. B **547**, 7 (2002)
40. J. Steinheimer, S. Schramm, H. Stöcker, Phys. Rev. C **84**, 045208 (2011)
41. F. Cooper, G. Frye, Phys. Rev. D **10**, 186 (1974)
42. P. Huovinen, H. Petersen, Eur. Phys. J. A **48**, 171 (2012)
43. J.K. Klay et al., Phys. Rev. Lett. **88**, 102301 (2002)
44. J.K. Klay et al., Phys. Rev. C **68**, 054905 (2003)
45. L. Ahle et al., Phys. Lett. B **476**, 1 (2000)
46. J. Steinheimer, J. Randrup, Phys. Rev. Lett. **109**, 212301 (2012)
47. P. Braun-Munzinger, J. Cleymans, H. Oeschler, K. Redlich, Nucl. Phys. A **697**, 902 (2002)
48. C. Alt et al., Phys. Rev. C **77**, 024903 (2008)
49. H. Petersen, M. Bleicher, Phys. Rev. C **81**, 044906 (2010)
50. C. Pinkenburg et al., Phys. Rev. Lett. **83**, 1295 (1999)
51. P. Danielewicz, R. Lacey, W.G. Lynch, Science **298**, 1592 (2002)
52. P. Hillmann, J. Steinheimer, M. Bleicher, J. Phys. G **45**, 085101 (2018)